2011 American Control Conference
on O'Farrell Street, San Francisco, CA, USA
June 29 - July 01, 2011

Generating images from non-raster data in AFM

Peng Huang and Sean B. Andersson
Department of Mechanical Engineering, Boston University, MA 02215

Abstract— **Non-raster methods in atomic force microscopy utilize high-level feedback control to steer the tip in order to sample only regions of interest. Although the non-raster method can reduce the scanning time by gathering fewer samples, the measurement locations are no longer uniformly distributed. As a result, the production of accurate images from the data is a non-trivial problem. This paper presents a method of generating images that faithfully represent the sample from the non-raster data based on Kriging spatial interpolation theory. The method is modified to work well with a particular non-raster method developed previously by one of the authors. One of the primary drawbacks of Kriging, however, is its computational cost. As the algorithm is too slow for real time use, we also describe the use Delaunay triangulation for image generation. While less accurate than Kriging, triangulation is fast enough to produce images in real time, providing visual feedback to the user during the image process.**

I. INTRODUCTION

The atomic force microscope (AFM) [1] is a versatile tool in nanoscience and nanotechnology, capable of imaging with nanoscale resolution both in ambient and liquid environments as well as in vacuum. The imaging rate of a conventional AFM, however, is typically on the order of minutes or more, depending on the resolution, scan range, and sample. This slow rate severely limits the ability of AFM to study dynamic processes. In order to address open questions ranging from surface diffusion, phase transition, film growth and etching, and biomolecular motors and processes [2], researchers are striving to decrease the imaging time while maintaining image quality. Approaches include improving the design of the mechanical components [2], [3], often combined with the use of high-speed data acquisition systems [4], and the use of modern control theory to drive the actuators as fast as possible [5], [6]. As a result of these efforts, video-rate imaging has been achieved [2] and the feasibility of using high-speed AFM to record fast processes in molecular biology has been demonstrated [7]–[9].

All of these approaches focus on improving the scan speed but continue to rely on the raster-scan sampling pattern. In many cases, however, the sample of interest is sparse in the image. As a result, most of the samples are of completely uninteresting substrate. Each of the data points on the sample represents wasted time. Non-raster methods seek to reduce the total number of samples by using the measured data in a feedback manner to drive the next sampling point. As high-level algorithms, non-raster methods are complementary to many of the high-speed AFM schemes. To date, the authors have focused primarily on non-raster schemes for imaging string-like samples such as biopolymers [10].

Under the raster scan pattern, the samples are evenly spaced and generation of images is straightforward. Under non-raster imaging, the acquired data is no longer regularly distributed in space. Therefore, generating images from the non-raster data is a non-trivial problem. Fig.1 illustrates the imaging results of a DNA sample of both raster and non-raster scan approaches. In order for the non-raster method to produce useful images, the data shown in Fig. 1(b) must be interpolated in such a way as to accurately capture the DNA with a fidelity similar to the raster image in Fig. 1(a). In choosing the spatial interpolation methods for reconstructing credible images by interpolating date onto a regular grid, accuracy is of primary concern.

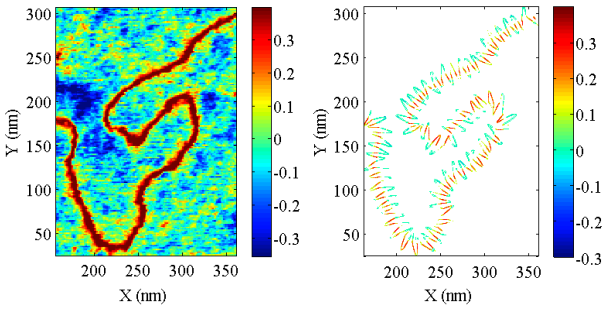

(a) Raster-scan (b) Non-raster scan

Fig. 1. Comparing raster to non-raster data. (a) Raster data (and image) of DNA. (b) Non-raster data set of the same DNA as the raster set. The challenge is to produce an image capturing the details of the DNA in (a) from the data set in (b). Note that the height unit is in nanometer.

Kriging models the data as the outcome of a random process and interpolates intermediate values using an unbiased estimator which has minimum variance over all unbiased linear estimators. Since the time cost of Kriging is quite high, it is best suited for off-line generation of images. It can be useful to the user, however, to have images produced in real time during the imaging process. We therefore also consider alternative methods that have lower accuracy but also lower computational complexity. A variety of methods exist, including polygonal interpolation, averaging, inverse distance methods, and triangulation. Among these, we focus on Delaunay triangulation since it is reasonably accurate but also computationally efficient.

This work was supported in part by the NSF through grant CMMI-0845742 and by a gift from Agilent Technologies.

II. A LOCAL RASTER SCAN APPROACH TO IMAGING STRING-LIKE SAMPLES

In this work we focus on producing images from non-raster data obtained by an algorithm developed by one of the authors for sampling biopolymers. We give here a brief overview of the scheme. Details can be found in [10], [12], [13].

On string-like samples such as biopolymers, the traditional raster scan image is primarily of uninteresting substrate. To avoid wasting time gathering useless data, we have designed a feedback controller that steers the tip to remain in close proximity to the underlying sample. Modeling the underlying sample as a planar curve, the measurements are used in real-time to estimate the curve parameters. This curve is in turn used to drive the tip trajectory according to

$$x_{tip}(t) = x_d(s(t)) + A\sin(2\pi fs)q_2(s(t)), \tag{1}$$

where $s(\cdot)$ is the arclength parameter of the curve representing the sample, $x_d(\cdot)$ is the estimated curve, $q_2(\cdot)$ is the estimated normal vector to the curve, A defines the amplitude of the scanning path, and f defines the spatial frequency and thus the resolution of the scanning. A sample run of the algorithm is shown in Fig.1 in which the algorithm was run in simulation on data captured in the traditional raster-scan mode.

III. KRIGING APPROACH

As an alternative approach to imaging in AFM, the non-raster scan should be capable of providing an imaging result as faithful as the conventional raster scan. Kriging is known as the best linear unbiased estimator [14] as it provides an estimation error with minimum variance. Kriging is more successful when it is well tuned to fit in the specific spatial distribution pattern of the given data. As a result, in the consideration of accuracy, Kriging becomes our first choice even though it bears high computational intensity.

Kriging performs interpolation using a weighted linear combination of the available data. The scheme views the sampled data as being generated by a random process. The weights are assigned to derive an unbiased approximation while minimizing the error variance. We give here a brief description of the algorithm. Details can be found in [15].

A. Overview

Kriging estimates the value at a target location S_0 according to

$$\hat{V}(S_0) = \sum_{i=1}^{n} \omega_i V(S_i), \tag{2}$$

where $S_1, \ldots, S_n$ are the positions with known values $V(S_i)$. The weights of this linear combination are computed by establishing a probabilistic model. In this model, $V(S_0), V(S_1), ..., V(S_n)$ are seen as the outcomes of first order stationary random processes with identical probability distributions. Therefore, the estimation error is also a random variable given by

$$R(S_0) = \sum_{i=1}^{n} \omega_i V(S_i) - V(S_0). \tag{3}$$

Accordingly, the mean and variance of the estimation error are calculated by

$$\begin{aligned} E(R(S_0)) &= E(\sum_{i=1}^{n} \omega_i V(S_i)) - E(V(S_0)) \\ &= E(V)(\sum_{i=1}^{n} \omega_i - 1), \end{aligned} \tag{4}$$

$$Var[R(S_0)] = \sigma^2 + \sum_{i=1}^{n}\sum_{j=1}^{n} \omega_i \omega_j C_{ij} + 2\sum_{i=1}^{n} \omega_i C_{i0}, \tag{5}$$

where σ^2 is the variance of V, $C_{ij} = C_{ij}(h)$, denotes the spatial covariance between the ith and jth points with respect to their distance h under our stationary assumption and $E(V)$ is the common mean of the random variables.

To achieve unbiasedness, set (4) to 0, yielding

$$\sum_{i=1}^{n} \omega_i = 1. \tag{6}$$

To minimize the error variance, apply the first order condition

$$\frac{\partial Var[R(S_0)]}{\partial \omega_i} = 0. \tag{7}$$

It can be shown that (7) yields n equations in the n unknown weights, $\omega_1, \omega_2, \ldots, \omega_n$. To enforce the unbiasedness condition in (6), introducing a Lagrange multiplier μ to enforce the unbiasedness condition. The optimal weights are then given by the following linear system.

$$\begin{bmatrix} C_{11} & \ldots & C_{1n} & 1 \\ \vdots & \ldots & \vdots & \vdots \\ C_{n1} & \ldots & C_{nn} & 1 \\ 1 & \ldots & 1 & 0 \end{bmatrix} \begin{bmatrix} \omega_1 \\ \vdots \\ \omega_n \\ \mu \end{bmatrix} = \begin{bmatrix} C_{10} \\ \vdots \\ C_{n0} \\ 1 \end{bmatrix}. \tag{8}$$

Let C denote the $(n+1)\times(n+1)$ matrix on the left of (8) and D the vector on the right. Under the assumption that the C matrix is invertible, the weights are given by

$$\omega = C^{-1}D. \tag{9}$$

This result indicates that the optimal choice of weights depends upon the C and D matrices. These are in turn constructed from $n(n+1)$ covariances that capture the spatial dependence of the data. In practice, they are typically calculated from standard covariance functions that guarantees the existence and uniqueness of the solution of (9). Then, a set of weights can be generated to produce unbiased estimates with minimum error variance subject to our accepted covariance function. If the chosen function happens to be inappropriate, that is, if it fails to capture the spatial continuity charac-

teristics of the data set, then Kriging is unable to offer a satisfying result. As a result, the successful application of Kriging requires the user to choose an appropriate covariance function, to inspect the resulting estimates, and to manipulate the model parameters until a satisfying interpolation is produced.

B. Challenges in our case

Several challenges arise when attempting to apply Kriging to the data sets acquired from non-raster scanning of biopolymers and other string-like samples.

The first challenge is due to the notion of distance in the samples. Since the AFM data is sampled over a 2-D region, a traditional interpretation would use a 2-D Euclidean distance. The actual sample, however, is essentially 1-D and the appropriate notion of distance is *along the sample*.

Second, the sample is highly anisotropic. The axis of continuity lies along the string and is constantly changing direction as the sample curves in space. As a result, a dynamic direction of anisotropy is needed. As it turns out, the local raster scan algorithm provides information as to the local axis of continuity due to the estimate of the local direction of the curve. Such information should be taken advantage of to produce good interpolation results.

Third, the time to generate images from the data set should be as small as possible. The Kriging algorithm is in general computationally intensive. As a result, it is important to employ an efficient algorithm for selecting relevant samples to use in the interpolation process and to select the smallest number of samples without reducing the quality of the interpolation. In particular, reducing the number of samples to use in each interpolation step is an effective means of decreasing the image generation time since the time cost is proportional to the cube of the number of the samples used [15].

Based on these considerations, we have modified the standard Kriging algorithm to take advantage of the particular data produced by our non-raster imaging algorithm.

C. Modified Kriging for string-like samples

1) Straightening out the sample: To motivate our modifications, consider the string-like sample in Fig. 2 (in red). The black dots in the figure represent discrete steps along the tip trajectory under the non-raster scan algorithm and the yellow dots indicate points at which the tip crosses the sample. The issue of finding relevant samples to use in the interpolation process is perhaps best illustrated by considering estimation at points between r_1 and r_2. The points at r_{1_1} through r_{2_6} certainly contain information relevant to the sample in that area. In standard Kriging, the point at r_N is also considered relevant since it is located within the neighborhood. However, the proximity of r_N is a consequence of the complex spatial evolution of the underlying sample and could even be on another sample entirely. In either case, the value at r_N has little to nothing to do with the height value of the samples near the points r_1 and r_2. Including the data at r_N in the interpolation process would skew the estimation, in this case leading to an erroneous widening of the sample. We therefore need to consider not Euclidean distance in the plane but rather distance in terms of arclength along the sample.

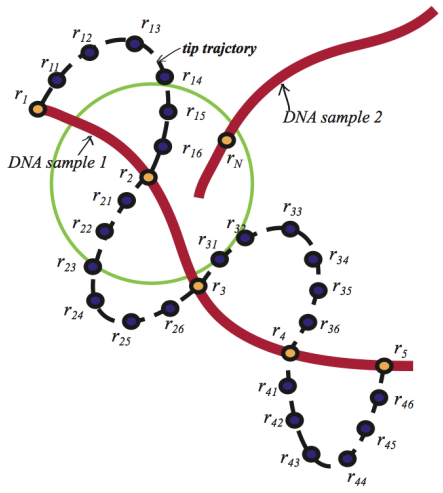

Fig. 2. A non-raster scan (black points) along a biopolymer sample (red). The crossing positions are highlighted in yellow. Point r_N, while physically near points r_1 through r_3, is not related to those points. Interpolation near r_1 through r_3 should therefore ignore r_N.

To do so, we straighten out the underlying sample trajectory. To first order, the sample trajectory between two crossings can be approximated by a straight line. Let r_j denote the crossing points and let r_{j_i} denote the planar position of the i^{th} point after the j^{th} crossing. To straighten the sample, we first calculate the transformation to straighten the segment between a pair of crossings. This transformation, denoted $\Phi\left(\cdot; r_j, \theta_{j,j+1}\right)$ is given by

$$\Phi\left(r_{j_i}; r_j, \theta_{j,j+1}\right) = T_{\theta_{j,j+1}}\left(r_{j_i} - r_j\right) + r_j, \tag{10}$$

where $\theta_{j,j+1}$ is the angle of the straight line connecting crossing points r_j and r_{j+1} with respect to the original lab-fixed frame and

$$T_\theta = \begin{bmatrix} \cos\theta & \sin\theta \\ -\sin\theta & \cos\theta \end{bmatrix} \tag{11}$$

is a rotation matrix.

The entire trajectory is then straightened as follows. Begin with r_1 and apply the transformation $\Phi(\cdot; r_1, \theta_{12})$ to all subsequent points. This will straighten out the portion between r_1 and r_2. Then move to $\Phi(r_2; r_1, \theta_{12})$ (the transformed position of r_2) and apply the transformation $\Phi(\cdot; \Phi(r_2; r_1, \theta_{12}) r_2, \theta_{23})$ to all subsequent points. This will yield a curve in which r_1, r_2,and r_3 are on a horizontal line (see Fig. 3). Continue in this pattern through all the points, yielding a transformed trajectory in which all the crossing points lie on a horizontal line. In these transformed

coordinates, the standard Euclidean distance describes the distance along the sample.

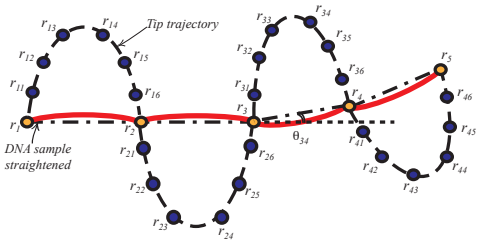

Fig. 3. The transformation $\Phi\left(\cdot; r_j, \theta_{j,j+1}\right)$ in (10) places the points r_j and r_{j+1} on a horizontal line. Applying the transformation sequentially yields a trajectory in which all the intersection points are on a horizontal line.

2) Defining the axis of anisotropy: When defining the spatial covariances in (8), it is important to capture the anisotropy in the spatial relationships between the data points. In standard Kriging, this is commonly done by having the variances differ in the different spatial directions. Such differences are typically uniform across the region to be interpolated.

In the data gathered by the local raster-scan algorithm, however, the local "direction" is again defined as along the sample. Thus it is constantly turning with respect to the lab frame, depending on the path defined by the sample. The local raster scan algorithm does record the heading direction at each crossing point. To account for this, we modify the covariances at every crossing point based on this information. Thus, the heading direction estimated by the local raster-scan algorithm at r_1 is used to define the direction of the covariances for interpolation between points r_1 and r_2 in Fig. 2, the heading direction at r_2 is used for points between r_2 and r_3, and so on.

3) Selecting points and reducing the interpolation time: The computational complexity of Kriging (for a single interpolation) has been shown to be in general given by [16]

$$T = A_0 + A_1 N + A_2 N^2 + A_3 N^3, \tag{12}$$

where T is the number of operations required (and thus proportional to the time needed), N is the number of the known samples being used in the interpolation, and A_0-A_3 are coefficients depending upon the hardware platform and the size of the image in terms of its area and resolution.

The most important factor in reducing the time to generate an image, then, is reducing the total number of points used in each interpolation event. Furthermore, since the substrate is nominally homogeneous, there is a large amount of redundancy in the measurements collected off of the sample. Finally, it is possible for the sample topology to change relatively rapidly along its length, especially if one is imaging proteins bound to biopolymers (such as polymerases on DNA or motor proteins on actin). When applying the Kriging algorithm, then, it is advantageous to take a small radius over which to use data in the interpolation.

In Sec. V, we apply our modified Kriging algorithm to a data set captured using the local raster-scan method. As discussed there, the time to generate a single image (using the DACE toolbox [17] in Matlab) is on the order of 40 s. While this time depends upon the hardware platform and the implementation of the code, it is clear that orders-of-magnitude improvement is needed for the method to be used for generating images at video rate speeds. While we are pursuing approaches to further reduce the computation time, here we assume Kriging will be used for off-line image generation. Since it can be quite useful to a user to see images in real time, in the next section we propose to use Delaunay triangulation, trading off some amount of accuracy for a more efficient computation.

In practice, effective use of Kriging will rely on some *a priori* knowledge of the sample. Knowing that the sample is DNA, for example, will help the user to choose the Kriging parameters and to evaluate the resulting image in terms of its gross structure. As with any imaging scheme, even with the standard raster scan method, the user must be aware of artifacts arising from the imaging process.

IV. Delaunay Triangulation Approach

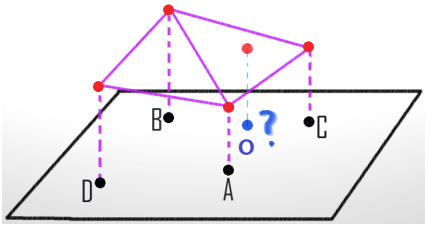

Fig. 4. Delaunay triangulation interpolates by creating a triangular mesh based on the available data.

Delaunay triangulation uses three nearby points to interpolate sample values based on a criterion, discussed below, that offers a smooth solution. It is a well-studied approach and well-tuned algorithms exist which enable it to run extremely quickly [18] [19]. Since only three points are used, the images produced in general have less accuracy than those made by Kriging but the speed of execution makes it a viable alternative for online implementation.

As shown in Fig. 4, to estimate the height value of the target position (denoted by the blue dot), triangulation employs the Delaunay criteria to build a triangular hull using a choice of three nearby known values (red dots) surrounding the target and their corresponding position coordinates (black dots). The edges of the hull are illustrated by the pink lines. The interpolated value at the target position is then given by the height on the triangular facet. Specifically, in the example shown, the value at O is given by

$$\hat{V}(S_0) = \frac{A_{OBC}V_A + A_{OAB}V_C + A_{OAC}V_B}{A_{ABC}}, \tag{13}$$

where A represents the area of the triangle defined by the points denoted in the subscript and V denotes the sample

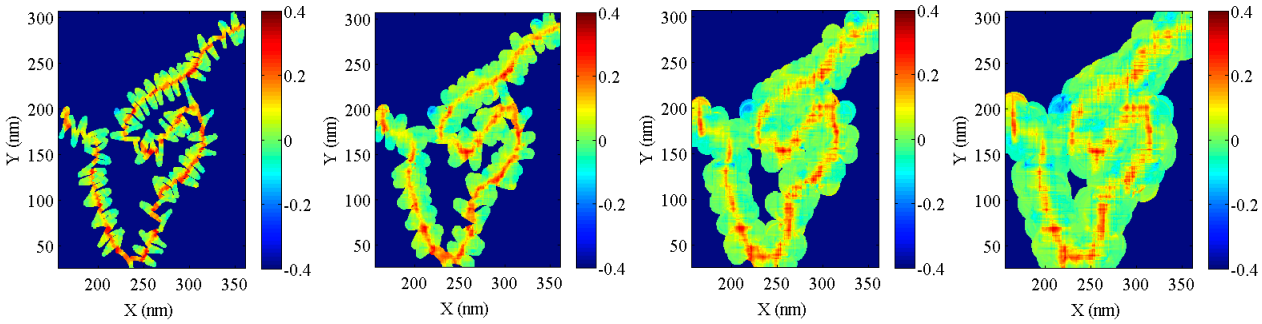

(a) radius = 15nm (b) radius = 33nm (c) radius = 66nm (d) radius = 100nm

Fig. 5. Kriging images based on different search radius (height is in the same arbitrary units as the original raster image).

value at the point denoted in the subscript. While there are many ways to generate a triangular mesh over a set of points, Delaunay creates a unique solution by finding one that maximizes the minimum angle of each triangle [11].

V. Simulation

To illustrate and evaluate the modified Kriging and Delaunay triangulation schemes, we applied both schemes to data sets acquired using the local raster scan algorithm operated in simulation on the regular raster scan image of DNA (see Fig. 1). The original data set (acquired in intermittent contact mode using an Asylum Research MFP-3D) had a spatial resolution of approximately 2.9 nm/pixel and was viewed as "ground truth". The accuracy of an interpolated image was described using the root mean square error on a pixel-by-pixel basis

$$RMS = \sqrt{\frac{\sum_{i=1}^{N} (\hat{x}_i - x_i)^2}{N}}, \tag{14}$$

where $\hat{x}_i$ denotes the estimated value in pixel i, x_i is the corresponding value in the raster result and N is the total number of estimations.

A. Low resolution data set

In the first simulation, we used a non-raster data set of 1767 samples along a 731 nm long DNA strand. The spatial resolution in this set (defined by the average spacing of the crossing points along the strand) was 17.4 nm. We applied our modified Kriging algorithm with four different search radii of (100, 66, 33, 15) nm. The resulting images are shown in Fig. 5. We also applied the Delaunay algorithm to the same data; the resulting image is shown in Fig. 6

In Table I we show the RMS error in the generated images and the time to compute the image. Among the Kriging images, the computation time is greatly reduced as the radius is reduced due to the smaller number of points used in the interpolation. With too large of a radius, points are used in the interpolation that are physically unrelated, leading to a larger RMS error. With too small of a radius, not enough points are used, also leading to a larger RMS error. In this data, a search radius of approximately twice the resolution in the data yielded the lowest image error. With a proper choice of the searching radii, kriging is capable of representing the profile of the sample well even when the spatial resolution of a given data set is not high. By comparison, the Delaunay image had a much larger error the algorithm executed approximately two orders of magnitude faster than Kriging.

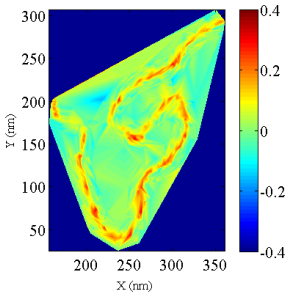

Fig. 6. Image generated using Delaunay triangulation from 1767 samples. The result should be compared to those based on Kriging in Fig. 5.

TABLE I
Results comparison, the red cell is the designed radius result

Radius (nm)	RMS (nm)	CPUTime (s)
100	0.09144	233.33
66	0.08912	107.59
33	0.00868	40.18
15	0.9928	20.24
Delaunay	0.2640	0.2

B. High resolution data set

The accuracy of an image is limited by the resolution of the original data set. To illustrate this, we performed image interpolation from data sets with 2701 and 5101 samples over the same range of the DNA. The imaging results based on Kriging (using a radius of twice the sampling resolution in the data set) are shown in Fig, 7. While the radius was

smaller in the higher resolution data, the number of points inside the radius remained approximately the same. As a result, the computation time remained approximately 40 s.

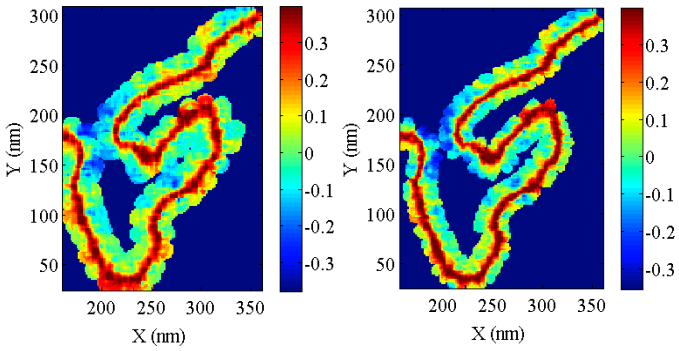

(a) 2701 samples result (b) 5101 samples result

Fig. 7. Fig.1(a) is the original raster scanning result; (a) is a kriging interpolation result of 2701 samples with lower spatial resolution than the data set in (b) of 5101 samples. The RMSs are 0.001418 and 0.0007112.

The same data sets were used in the Delaunay algorithm. The resulting images are shown in Fig. 8. While the images capture the gross structure of the DNA with RMSs as low as Kriging results, there are more artifacts. We note that since Delaunay uses only three local points in the interpolation, it is relatively straightforward to speed up the algorithm by building the image a small region at a time based on small blocks of incoming data. Note that for these high-resolution data sets, the RMS error for the Delaunay images were comparable to those of the Kriging images, indicating the faster algorithm is as effective given enough data. The images, however, do show clear artifacts, such as "filling in" regions where no data was acquired. Such artifacts can be misleading to the user.

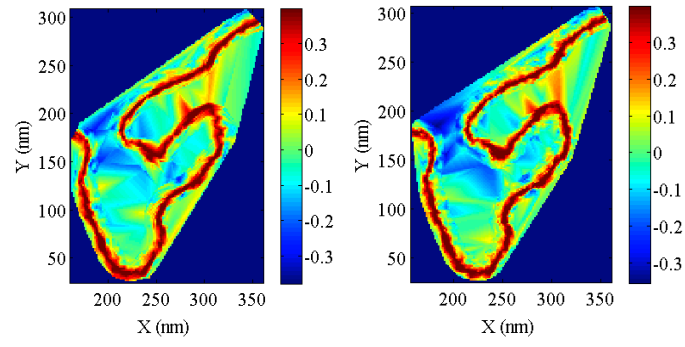

(a) 2701 samples result (b) 5101 samples result

Fig. 8. Delaunay interpolation based on (a) 2701 and (b) 5101 samples. The RMSs are 0.001316 and 0.0007685.

VI. CONCLUSIONS

We have presented a modified Kriging algorithm and compared it to Delaunay triangulation for the generation of images from a non-raster scan algorithm designed for high-speed imaging of biopolymers and other string-like samples. The results indicate that our Kriging method yields more accurate images but at a high computational cost. It is therefore best suited for offline image generation. Delaunay, while less accurate, is fast enough for real-time implementation.

REFERENCES

[1] G. Binnig and C.F. Quate, "Atomic force microscope," *Phys. Rev. Lett.*, vol. 56, no. 9, pp. 930–933, March 1986.

[2] G. Schitter and M. J. Rost, "Scanning probe microscopy at video-rate," *Mat. Today*, vol. Microscopy special issue, pp. 40–48, 2008.

[3] G. E. Fantner, G. Schitter, J. H. Kindt, T. Ivanov, K. Ivanova, R. Patel, N. Holten-Andersen, J. Adams, P. J. Thurner, I. W. Rangelow, and P. K. Hansma, "Components for high speed atomic force microscopy," *Ultramicroscopy*, vol. 1, no. 15, pp. 1–7, Jan 2004.

[4] G. E. Fantner, P. Hegarty, J. H. Kindt, G. Schitter, G. A. G. Cidade, and P. K. Hansma, "Data acquisition system for high speed atomic force microscopy," *Rev. Sci. Inst.*, vol. 76, no. 2, pp. 76–79, Jan 2004.

[5] G. Schitter, F. Algöwer, and A. Stemmer, "A new control strategy for high-speed atomic force microscopy," *Nanotech.*, vol. 15, pp. 108–114, Nov 2004.

[6] S. Salapaka, A. Sebastian, J. P. Cleveland, and M. V. Salapaka, "High bandwidth nano-positioner: A robust control approach," *Rev. Sci. Inst.*, vol. 73, no. 9, pp. 3232–3241, Sep 2002.

[7] A. U. L M Picco, L Bozec, D. J. Engledew, M. Antognozzi, M. A. Horton, and M. J. Miles, "Breaking the speed limit with atomic force microscopy," *Nanotech.*, vol. 18, pp. 1–4, Dec 2006.

[8] M. B. Viani, L. I. Pietrasanta, J. B. Thompson, A. Chand, I. C. Gebeshuber, J. H. Kindt, M. Richter, H. G. Hansma, and P. K. Hansma, "Probing protein–protein interactions in real time," *Nat. Struct. Bio.*, vol. 7, no. 8, pp. 644–647, Aug 2000.

[9] T. Ando, T. Uchihashi, N. Kodera, D. Yamamoto, A. Miyagi, M. Taniguchi, and H. Yamashita, "High-speed afm and nano-visualization of biomolecular processes," *Eur. J. Physiol.*, vol. 456, pp. 211–225, Dec 2008.

[10] S. B. Andersson, "Curve tracking for rapid imaging in afm," *IEEE Trans. Nanobio.*, vol. 6, no. 4, pp. 354–361, Dec 2007.

[11] *Voronoi diagrams and Delaunay Triangulations*, E. H. Isaaks and R. M. Srivastava ed, World Scientific, 1992, pp. 193–233.

[12] P. I. Chang and S. B. Andersson, "Smooth trajectories for imaging string-like samples in AFM: A preliminary study," in *Proc. of the American Control Conference*, June 2008, pp. 3207–3212.

[13] ——, "A maximum-likelihood detection scheme for rapid imaging of string-like samples in atomic force microscopy," in *Proc. of the IEEE Conference on Decision and Control*, June 2009, pp. 8290–8295.

[14] M. L. Stein, *Interpolation of Spatial Data*. Springer, 1999.

[15] E. H. Isaaks, *Applied Geostatistics*. Oxford University Press, 1989.

[16] K.E.Kerry and K.A.Hawick, "Kriging interpolation on high-performance computers," *Technical Report*, no. DHPC-035.

[17] N. Lophaven, H. B. Nielsen, and Jacob, "Dace, a Matlab Kriging toolbox," *Inf. Math. Modelling*, Aug 2002.

[18] D. Lischinski, "Incremental Delaunay triangulation," *Academic Press*, 1993.

[19] D. T. Lee and B. J. Schachter, "Two algorithms for constructing a Delaunay triangulation," *Int. J. Parallel Prog.*, vol. 9, no. 3, June 1980.